Modeling InGaN Disk-in-Wire LEDs: Interplay of Quantum Atomicity and Structural Fields

Krishna Yalavarthi, Vinay Chimalgi, Sasi Sundaresan and Shaikh Ahmed, *Member, IEEE*
Department of Electrical and Computer Engineering
Southern Illinois University at Carbondale,
1230 Lincoln Drive, Carbondale, IL 62901, USA, E-mail: ahmed@siu.edu

***Abstract*—The objective of this paper is to study how quantum efficiency of *nanostructured* GaN/InGaN/GaN disk-in-wire LEDs is determined by an intricate interplay of atomicity of the wurtzite crystal symmetry, structural relaxation and induced piezoelectric field, built-in spontaneous polarization, and carrier dynamics, recombination, and relaxation processes. We have employed a multiscale approach where: (i) the long-range *mechano-electrical* internal fields in the structure have been modeled using a combination of an *atomistic* valence force-field molecular mechanics (VFFF MM) approach and a three-dimensional Poisson solver; (ii) the one-particle electronic states and optical transition rates have been determined using a 10-band sp^3s^* tight-binding framework; and (iii) the Synopsys TCAD tool, coupled with the microscopically determined parameters, is then used to obtain the terminal electrical and optical properties of the device. It is found that internal fields in these nanostructured LEDs lead to pronounced optical anisotropy and suppression in the interband optical transitions (near the center of the Brillouin zone) and, therefore, strongly affect the conversion efficiency. Lastly, to identify the optimum LED structure, we considered $In_xGa_{1-x}N$ active region with varying Indium concentration, for which the internal quantum efficiency (IQE) was determined.**

***Index Terms*—III-nitride LEDs, optical polarization, strain, piezoelectricity, spontaneous polarization, tight-binding.**

I. Introduction

In the last decade, GaN and its related alloys, especially InGaN, have been viewed as the most promising materials for high performance light-emitting diodes (LEDs), with emission wavelengths in the green, yellow and red spectral range [1][2]. LEDs based on wide-bandgap InGaN semiconductors could be used in such applications as lasers, solid-state lighting, solar cells, consumer displays, as well as diagnostic medicine and biological imaging.

Majority of the experimental work on nitride material system is currently focused on wurtzite polar oriented (*c*-plane), two-dimensional quantum well (QW) structures. However, the performance of these planar structures is limited by [3]: (i) the pronounced non-radiative recombination rate induced by the quantum confined Stark effect due to spontaneous and piezoelectric polarizations, and (ii) the high density of non-radiative defects due to the increasing lattice mismatch between GaN and InGaN alloys with higher In content. To combat these challenges, in recent times, *nanostructured* disk-in-wire structures [3][4][5] have caught researcher's attention. In these devices, improved electron confinement (due to strongly peaked energy dependence of density of states) coupled with the fact that the concentration of strain-induced defects is lower in nanostructures allow for the use of *higher* indium content in the device, which potentially could lead to *full-spectrum* LEDs (as well as solar cells).

Befitting investigation of electronic bandstructure of nanostructures is a prior requirement towards understanding the optical performance and reliability of these reduced dimensionality III-N LEDs. These structures are subject to internal structural and electrostatic fields originating from: (i) the fundamental crystal atomicity and the interface discontinuity between two dissimilar materials, (ii) atomistic strain relaxation, (iii) piezoelectricity, and (iv) spontaneous polarization. The magnitude of the electrostatic built-in field has been estimated to be on the order of MV/cm. Such fields spatially separate the electrons and holes, which leads to a reduction in the optical transition rate (oscillator strength) and enhanced radiative lifetimes. Therefore, electronic and optical properties of these nanostructures are expected to be strong functions of an intricate interplay between the atomistic structural fields and the quantum mechanical size quantization. Despite recent progress in nitride material systems and structures, experiments on optical properties of thin InGaN nanowires are scarce and, therefore, demand detailed theoretical investigations.

II. Simulation Model

The overall simulation strategy is divided into five coupled computational phases: a) geometry construction, b) structural (strain) relaxation, c) computing the *long-range* internal fields, d) determining the *atomistic* electronic structure and optical transitions, and e) integrating the atomistically calculated transition rates to a commercial TCAD tool (Synopsys). The purpose of the geometry constructor is to create (from a basis set) the nanostructure having wurtzite symmetry and to store the atomistic details (type, coordinates, nearest neighbors, surface passivation, and computation type). Initially, the atom positions in the entire computational domain (including those of InN) are fixed to the GaN lattice constant. Then, the atom positions are relaxed and the resulting strain (mechanical) fields are calculated employing an atomistic valence force-field (VFF) method using the Keating potentials. In this approach, the total elastic energy of the sample is computed as a sum of bond-stretching and bond-bending contributions from each atom. Next, the calculation of the internal fields is carried out. The overall polarization $\mathbf{P}$ in a typical wurtzite semiconductor is given by $\mathbf{P} = \mathbf{P}_{PZ} + \mathbf{P}_{SP}$, where

This work is supported by National Science Foundation Grant No. 1102192. Access to the ORNL computing resources through the ORAU High-Performance Computing Grant 2009 and Synopsys TCAD tools are also acknowledged.

 ISBN 978-0-615-71756-2

$\mathbf{P}_{PZ}$ is the strain-induced piezoelectric polarization and $\mathbf{P}_{SP}$ is the spontaneous polarization (pyroelectricity). The piezoelectric polarization $\mathbf{P}_{PZ}$ is obtained from the diagonal and shear components of the anisotropic *atomistic* strain fields. In contrast, the spontaneous polarization is strain-independent and arises from fundamental asymmetry of the crystal structure. The polarization induced *charge density* is derived by taking divergence of the polarization. To do this, we divide the simulation domain into cells by rectangular meshes. The polarization of each *grid* is computed by taking an average of atomic polarization within each cell. A finite difference approach is then used to calculate the charge density by taking divergence of the grid polarization. Finally, the induced potential is determined by the solution of the 3-D Poisson equation on an atomistic grid (using an in-house PETSc-based parallel full 3-D Poisson solver). The strain parameters and polarization constants used in this work are taken from Ref [6]. Next, the single-particle energies and wave functions are calculated using an empirical nearest-neighbor 10-band sp^3s^* tight-binding model. For this purpose we have augmented the open source NEMO 3-D tool and used the computational framework available therein. Detail description of this package can be found in Ref. [7][8]. The tight binding parameters for GaN and InN are taken from [9]. Finally, the *spontaneous* optical emission (absorption) rate is calculated using [10]:

$$R\left(k_i,k_f,E\right)=\frac{2\pi}{\hbar}\frac{q^2A^2}{4m_0^{\,2}}\left|\vec{M}_{cv}\left(k_i,k_f\right)\cdot\hat{n}\right|^2\times \delta\left[E_v\left(k_f\right)-E_c\left(k_i\right)+E\right]\times F, \quad (1)$$

where, $\vec{M}_{cv}$ is the momentum (optical) matrix calculated from the overlap of HOMO (valence) and LUMO (conduction) wavefunctions and F is the probability of hole occupation and electron vacancy, given by:

$$\vec{M}_{cv}\left(k_i,k_f\right)=\oint_{\Omega}d^3r\psi^*_{c,k_i}\left(r\right)\frac{\hbar}{j}\vec{\nabla}\psi_{v,k_f}\left(r\right), \quad (2)$$

$$F=f\left(E_v\left(k_f\right)-E_{fh}\right)\times\left[1-f\left(E_c\left(k_i\right)-E_{fe}\right)\right]. \quad (3)$$

When F = 1, emission (absorption) rate solely depends on the momentum matrix, where *absorption* and *emission* lose their meaning and we use a term *transition rate*. Note that for non-periodic finite-sized nanostructures (such as quantum disks), to calculate $\vec{M}_{cv}$, one needs to integrate in the entire domain. Since no free wave is available in a quantum disk, $k_i=k_f=0$ is the only available point used in the calculation.

To determine the terminal electrical and optical properties, we have used Synopsys's TCAD tools namely, Sentaurus Structure Editor, Sentaurus Device, and Tecplot or Inspect. Sentaurus Device includes models for the comprehensive simulation of LEDs, which solves drift-diffusion or hydrodynamic transport equations for the carriers, the Schrödinger equation for gain in the active optical and optical rate equations, and the Helmholtz equations self-consistently in the quasi-stationary and transient modes. Photon recycling is another important model used to predict the light trapping in the device by total internal reflection.

III. Simulation Results

Figure 1 illustrates the simulated disk-in-wire LED. The core active region of the device comprises of an undoped 10-nm thick $In_{0.16}Ga_{0.84}N$ disk grown in the [0001] direction. The InGaN disk is sandwiched between an *n*-doped GaN buffer region and a *p*-doped GaN cap layer both having base length, *b*~10 nm and height, *h*~45 nm. The disk-in-a-wire system is grown on a 40-nm thick sapphire substrate (ignored in the atomistic simulation).

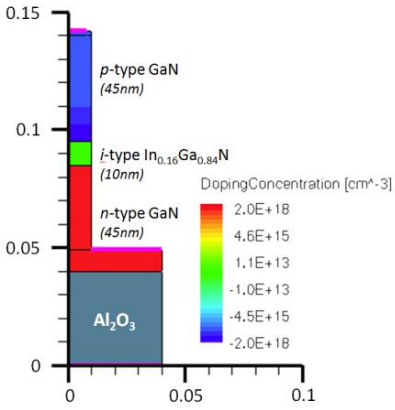

Figure 1. Simulated $In_xGa_{1-x}N$/GaN disk-in-wire LED structure. Also seen are the doping profiles of the buffer, disk and cap regions.

In the strain calculations, as shown in Figure 2, atomistic strain was found to be long-ranged, stressing the need for using realistically-extended structures (multimillion-atom modeling) in modeling electronic structure of these disks. The overall hydrostatic strain $\left(\varepsilon_{xx}+\varepsilon_{yy}+\varepsilon_{zz}\right)$ was found to be compressive within the $In_xGa_{1-x}N$ disk and tensile in the GaN buffer and cap layers. Lower panel in Figure 2 shows the off-diagonal strain distributions in the [0001] direction through the center of the disk. The *inequivalence* of ε_{xz} and ε_{yz} components arises from the rhombohedral geometry of the system.

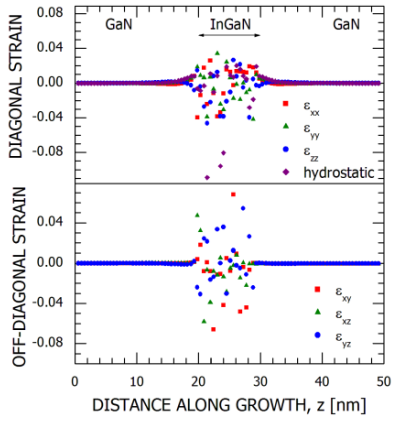

Figure 2. Atomistic strain along the growth ([0001]) direction through the center of the quantum disk. Strain is seen to penetrate into the substrate and the cap layers. Also, noticeable is the gradient of strain inside the quantum disk region.

In pseudomorphically grown heterostructures, the presence of non-zero atomistic stress tensors results in a deformation in the crystal lattice and leads to a combination of piezoelectric and pyroelectric fields. The polarization-induced potential is calculated using a parallel full 3-D Poisson solver and shown in Figure 3. Both the piezoelectric and the pyroelectric potentials are found to be long-ranged, significantly large and anisotropic in the lateral and vertical planes (bottom panel). However, the noticeable fact is that the piezoelectric potential is larger in magnitude and opposite in direction when compared to its pyroelectric counterpart.

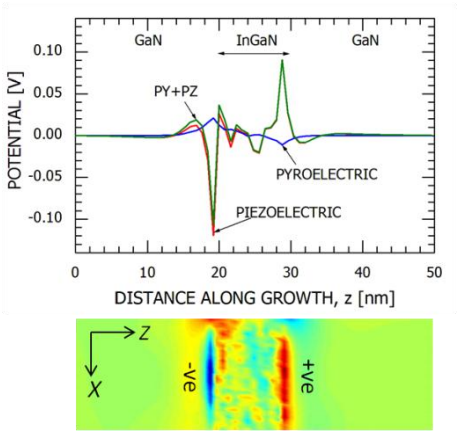

Figure 3. (top) Polarization induced potential along the [0001] direction. Note the large spread of the potential in the substrate and the cap layers. (bottom) Potential distribution in the XZ plane halfway through the width including both piezoelectric and pyroelectric contributions.

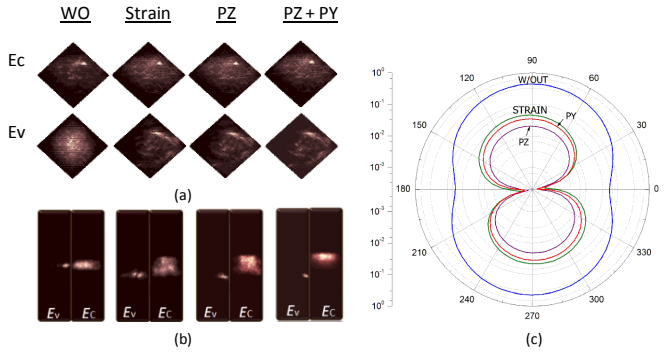

Figure 4. Electronic wavefunctions and optical transitions as a function of interface effects (w/out strain), strain, piezoelectricity, and pyroelectricity. Left panel (a and b) shows the HOMO and LUMO wavefunctions projected on the XY and XZ planes. Right panel (c) shows the polar plots of the in-pane interband optical transition rates between HOMO and LUMO in the quantum disk.

Next we calculate the *electronic structure* of the quantum disk. Here, we quantify the contributions of interface symmetry (W/out strain relaxation), strain, piezoelectricity, and pyroelectricity separately by computing the eigenvalues and wavefunction orientations. Figure 4 (a and b) illustrates the *localization* of HOMO and LUMO wavefunctions in the XY and XZ planes as a function of interface asymmetry/atomistic randomness, strain relaxation, piezoelectricity and pyroelectricity. Figure 4 (c) shows the polar plots of the interband optical transition rates between HOMO and LUMO in $In_{0.16}Ga_{0.84}N$ quantum disk projected on the XY plane. The Figure reveals significant suppression (by several orders of magnitude) and strong polarization anisotropy in the optical emission especially due to spatial irregularity and rotation in the wavefunctions. The true atomistic symmetry coupled with the quantum size quantization in the disk-in-wire systems, thus, influences both the electronic bandstructure and optical properties.

It is important to note that the electronic structure of $In_xGa_{1-x}N/GaN$ disk in wire system strongly depends on the *alloy composition* in the quantum disk region. Hence, in order to better ascertain the dependence on alloy composition, we performed simulations on varying mole fractions of InGaN in the active disk region. Figure 5 compares the bandgap energies (left panel) and transition rates (right panel) of the quantum disk by taking into account the *combined/net* effects of interface and atomistic symmetry, strain, piezoelectricity, and pyroelectricity as a function of varying In molar concentrations. This Figure exhibits a steady decrease in the bandgap energies as we move from lesser Indium concentration $x = 0.16$ to higher Indium concentrations ($x = 0.24, 0.40, 0.64, 0.84$). Figure 5 (left panel) also exemplifies a steady *red-shift* in the energy bandgap as we incorporate piezoelectricity in the structure, which is somewhat reduced by the pyroelectric counterpart. Also, from the polar plots (right panel), one can observe an invariant degradation in the *magnitude* and *isotropy* of optical transitions as we increase the In concentration. This characteristic can be attributed to the fact that the piezoelectricity is pronounced as a result of increased lattice mismatch and alloy randomness.

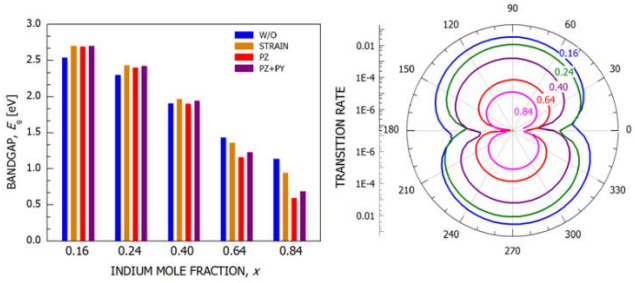

Figure 5. Bandgap (left) and the polar plots (right) of the interband optical transition rates between HOMO and LUMO in the quantum disk projected on the XY plane including interface effects (w/out strain), strain, piezoelectricity, and pyroelectricity as a function of alloy (In) composition.

The giant *in-plane* polarization anisotropy (defined by $r = \frac{|I_{max} - I_{min}|}{|I_{max} + I_{min}|}$) for emissions in the XY plane as a function of indium concentration is illustrated in Figure 6. The strong polarization anisotropy in the optical emission is especially due to spatial irregularity in the HOMO and LUMO wavefunctions which are shown as insets in Figure 6. Here, in contrast to the

huge variation observed in the *magnitude* of the trasition rates for varying alloy composition, the in-plane optical anisotropy of the system tends to be pronounced and consistent.

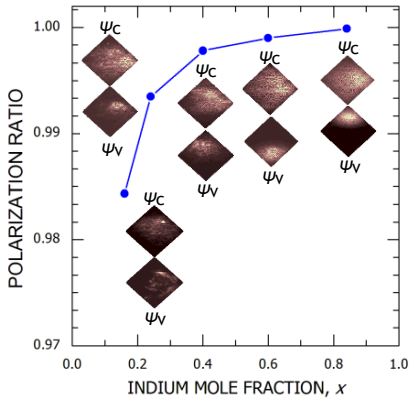

Figure 6. Growth-plane polarization anisotropy as a function of alloy (indium) concentration. The insets show the corresponding HOMO and LUMO wavefunctions in the XY plane.

Nest, we determine the optical properties of the device using the Synopsys's TCAD tool set. Here, we consider the device with Indium concentration of $x = 0.16$ since it exhibits the highest *average* optical transition rate. Figure 7 shows the internal quantum efficiency (IQE) of the $In_{0.16}Ga_{0.84}N$ disk-in-wire LED as a function of injected current at different levels of approximation. Here, the interface charges refer to polarization-induced charge density and K_{SP} defines the *correction factor* for the optical transition due to the presence of the internal fields. From our analysis, the large reduction of optical transition rates and giant anisotropy in the emission characteristics suggest that improved design of light-emitters in these III-nitride material systems would require novel nano-structured LEDs (such as disk-in-wire) and better compositional matching.

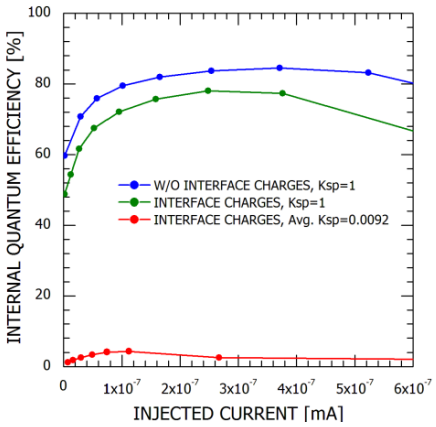

Figure 7. Internal quantum efficiency: (i) Without internal fields (blue); (ii) With polarization charges but assuming K_{SP} = 1 (green); and (iii) With polarization charges and realistic *average* K_{SP} = 0.0092 (red).

IV. Conclusion

$In_xGa_{1-x}N$ nanostructures are excellent candidates for white light emitters. Electronic and optical properties of these reduced-dimensionality devices are strongly influenced by an intricate interplay of internal fields, electronic bandstructure effects, charge and phonon transport, and randomness due to alloy composition. Internal fields are long-ranged and atomistic in nature, which necessitates the need for using realistically-extended substrate and cap layers containing millions of atoms in the computational domain. Internal fields result in: a) large red-shift in bandgap (quantum confined stark effect) as compared to the bulk value; b) pronounced degradation in transition rate; and c) reduced quantum efficiency and anisotropic emission spectra. In particular, piezoelectric polarization is very strong in InGaN disk-in-wire systems. Alleviating the strain by decreasing the Indium concentration proves to be instrumental in improving the optical performance of these nanoscale light-emitters.

Acknowledgment

This work is supported by the National Science Foundation Grant No. ECCS-1102192. Computational resources supported by the ORAU/ORNL High-Performance Computing Grant 2009 and access to the Synopsys TCAD toolset are acknowledged. Currently, the open source NEMO 3-D code is being maintained by Gerhard Klimeck at Purdue University. Discussion with Muhammad Usman and Hoon Ryu is also acknowledged.

References

[1] F. Ponce and D. Bour, "Nitride-based semiconductors for blue and green light-emitting devices," *Nature*, vol. 386. pp. 351–359, 1997.

[2] H. Morkoç and S. Mohammad, "High-luminosity blue and blue-green gallium nitride light-emitting diodes," *Science*, vol. 267, pp. 51–55, 1995.

[3] S. Albert, A. Bengoechea-Encabo, P. Lefebvre, F. Barbagini, M. A. Sanchez-Garcia, E. Calleja, U. Jahn, and A. Trampert, "Selective area growth and characterization of InGaN nano-disks implemented in GaN nanocolumns with different top morphologies," *Appl. Phys. Lett.*, vol. 100, 231906, Jun. 2012.

[4] Y. Lu, H. Lin, H. Chen, Y-C. Yang, and S.Gwo, "Single InGaNnanodisk light emitting diodes as full-color subwavelength light sources," *Appl. Phys. Lett.*, vol. 98, 233101, 2011.

[5] H. P. T. Nguyen, S. Zhang, K. Cui, X. Han, S. Fathololoumi, M. Couillard, G. A. Botton, and Z. Mi, "*p*-Type Modulation Doped InGaN/GaN Dot-in-a-Wire White-Light-Emitting Diodes Monolithically Grown on Si(111)," *Nano Lett.*, vol. 11, no. 5, pp 1919–1924, 2011.

[6] T. Saito, Y. Arakawa, "Electronic structure of piezoelectric $In_{0.2}Ga_{0.8}N$ quantum dots in GaN calculated using a tight-binding method", *Physica E: Low-Dimensional Systems and Nanostructures*, vol. 15, pp. 169–181, 2002.

[7] G. Klimeck, S. Ahmed, N. Kharche, H. Bae, S. Clark, B. Haley, S. Lee, M. Naumov, H. Ryu, F. Saied, M. Prada, M. Korkusinski, and T. Boykin, "Atomistic Simulation of Realistically Sized Nanodevices Using NEMO 3-D", *IEEE Trans. Electron Devices*, vol. 54, 9, pp. 2079–99, 2007.

[8] S. Ahmed, S. Islam, and S. Mohammed, "Electronic Structure of InN/GaN Quantum Dots: Multimillion Atom Tight-Binding Simulations", *IEEE Trans. Electron Devices*, vol. 57, 1, pp. 164–173, 2010.

[9] N. Baer, S. Schulz, S. Schumacher, P. Gartner, G. Czycholl, and F. Jahnke, "Optical properties of self-organized wurtzite InN/GaN quantum dots: A combined atomistic tight-binding and full configuration interaction calculation", *Appl. Phys. Lett.*, vol. 87, 231114, 2005.

[10] E. F. Schubert, *Light-Emitting Diodes*, 2nd ed. University Press: Cambridge, 2008.